Geophysical Research Letters

RESEARCH LETTER
10.1029/2024GL111793

In Situ Observational Evidence of the Polar Cap Arc at 1500 MLT (15MLT-PCA) Associated With the Lobe Reconnection

Huiting Feng[1], Desheng Han[1], Shangchun Teng[2], Huixuan Qiu[1], Su Zhou[3], Run Shi[1], and Yongliang Zhang[4]

[1]State Key Laboratory of Marine Geology, School of Ocean and Earth Science, Tongji University, Shanghai, China, [2]Department of Earth Sciences, the University of Hong Kong, Pokfulam, China, [3]School of Science, Guiyang University, Guiyang, China, [4]The Johns Hopkins University Applied Physics Laboratory, Laurel, MD, USA

Key Points:

- The observations show that the occurrence of 15MLT-PCA was accompanied by FTEs on the dusk flank of the southern hemisphere's magnetopause
- The 15MLT-PCA is accompanied by an enhancement of upward FACs and an increase in sunward plasma flow near its root
- We provided evidence that the 15MLT-PCA results from lobe reconnection occurring at duskside boundary of the cusp

Supporting Information:

Supporting Information may be found in the online version of this article.

Correspondence to:

D. Han,
handesheng@tongji.edu.cn

Citation:

Feng, H., Han, D., Teng, S., Qiu, H., Zhou, S., Shi, R., & Zhang, Y. (2024). In situ observational evidence of the polar cap arc at 1500 MLT (15MLT-PCA) associated with the lobe reconnection. *Geophysical Research Letters*, *51*, e2024GL111793. https://doi.org/10.1029/2024GL111793

Received 2 AUG 2024
Accepted 5 NOV 2024

Author Contributions:

Conceptualization: Huiting Feng, Desheng Han, Shangchun Teng, Su Zhou
Data curation: Huiting Feng, Huixuan Qiu, Su Zhou, Run Shi, Yongliang Zhang
Formal analysis: Shangchun Teng, Huixuan Qiu
Funding acquisition: Desheng Han, Shangchun Teng, Su Zhou
Investigation: Huiting Feng
Methodology: Huiting Feng, Desheng Han, Shangchun Teng, Huixuan Qiu, Su Zhou, Run Shi
Project administration: Desheng Han
Resources: Huiting Feng
Software: Huiting Feng

Abstract The polar cap arc at 1500 MLT (15MLT-PCA) has been considered as an auroral signature of the cusp's duskside boundary and been speculated to be caused by lobe reconnection. However, no observational evidence has been provided to support this speculation. Here we report a 15MLT-PCA event occurred on 29 November 2017 using multi-instrument observations. During the DMSP observed the 15MLT-PCA, Cluster, with its footprints at the root of the 15MLT-PCA, identified two FTEs in the southern hemisphere's lobe region, accompanied by an increase in electron and ion energy from hundreds of eVs to several keVs. AMPERE observed an increase in upward field-aligned currents associated with the 15MLT-PCA. SuperDARN observed a single cell convection with an enhancement of sunward plasma flow near the root of 15MLT-PCA. We suggest that these observations provide the in-situ observational evidence that the 15MLT-PCA is generated by a lobe reconnection at the cusp's duskside boundary.

Plain Language Summary Auroras primarily occur within an oval-shaped region centered on Earth's magnetic poles. Under specific conditions, they can also occur within the polar cap, where auroral structures usually appear as arc-like or spot-like. Auroras exhibiting arc-like structures in this region are collectively termed polar cap auroral arcs (PCA). One such common phenomenon is the 15 magnetic local time-polar cap arc (15MLT-PCA), typically observed near the 1500 MLT sector in the summer hemisphere, extending from the poleward boundary of the auroral oval to the pole. Additionally, its occurrence shows a strong dependence on the B_y component of the interplanetary magnetic field (IMF). It is widely accepted that the generation of north-south asymmetric auroral structures in the polar cap results from reconnection between the IMF and Earth's magnetic field lines at high latitudes. Based on the observational characterization of 15MLT-PCA, it is currently believed that this structure is associated with lobe reconnection. However, direct in situ observational evidence for this process is currently lacking. Therefore, in this study, we combined ionospheric and magnetospheric satellites to validate a possible magnetospheric process for 15MLT-PCA.

1. Introduction

Most auroras occur in oval-shaped bands around the magnetic poles, known as auroral ovals (Feldstein, 1990; Feldstein et al., 1969). A smaller portion appears in the polar caps, surrounded by the poleward edges of the auroral oval (Hosokawa et al., 2020). Polar cap auroras are primarily classified into arc-shaped and spot-shaped structures based on their optical features (Hosokawa et al., 2020; Kullen et al., 2015; Zhang et al., 2016). One typical type of dayside polar cap auroras is the High-Latitude Dayside Auroras (HiLDAs), which have been explored in relatively few studies (Cai et al., 2021; Carter et al., 2018; Feng et al., 2021; Frey, Immel, et al., 2003, 2004; Han et al., 2020; Zhang et al., 2021). HiLDAs are further categorized into spot-like and arc-like structures (e.g., Cai et al., 2021; Frey, Immel, et al., 2003, 2004). The arc-like HiLDAs is also defined as 15MLT-PCA (Han et al., 2020), and we will use this term throughout the paper to describe this structure. Spot-like HiLDAs occur between 0600 MLT and 1900 MLT, peaking at 1500 MLT. These are mainly observed during sunlit months under IMF conditions with positive B_z, positive B_y, and negative B_x components in the northern hemisphere (Frey, Immel, et al., 2003). The 15MLT-PCA also happens in the sunlit hemisphere, showing dependence on universal time (UT) and the solar cycle (Han et al., 2020). Compared to the spot-like HiLDAs, it appears as a stable arc-like structure near the 1500 MLT sector of auroral oval, extending almost vertically into the polar cap (Han et al., 2020). The occurrence of 15MLT-PCA predominantly depends on IMF B_y and less on IMF B_z. Long-term

Supervision: Desheng Han, Shangchun Teng
Validation: Huiting Feng
Visualization: Huiting Feng
Writing – original draft: Huiting Feng
Writing – review & editing: Huiting Feng, Desheng Han, Shangchun Teng, Huixuan Qiu, Run Shi

observations from the Special Sensor Ultraviolet Spectrographic Imager (SSUSI) on the Defense Meteorological Satellite Program (DMSP) indicate that 15MLT-PCA mainly occurs under prolonged and stable positive IMF B_y and predominant negative IMF B_x conditions in the northern hemisphere (Han et al., 2020), with opposite favorable IMF conditions in the southern hemisphere (Feng et al., 2021). Additionally, the 15MLT-PCA usually observed in the transitional region of nightside central plasma sheet or boundary plasma sheet and the cusp or low-latitude boundary layer, and has been suggested to occur at the duskside of cusp (Feng et al., 2022).

Magnetic reconnection is a fundamental process where magnetic field lines with anti-parallel components reconnect. This process releases magnetic energy into plasma kinetic energy (Yamada et al., 2010). This phenomenon occurs throughout solar-terrestrial space, including during solar flares, at the magnetopause, and in the magnetotail (e.g., Angelopoulos et al., 2020; Dungey, 1961). Unsteady, patchy, or intermittent magnetic reconnection processes can lead to the formation of flux ropes, commonly observed as flux transfer events (FTEs). The distinctive features of FTEs resulting from reconnection are as follows (Marchaudon et al., 2005; Russell & Elphic, 1979): (a) a bipolar signature of B_N component with an increase of B_L component and total magnetic field ($|B_T|$); (b) an increase (decrease) in electron density (N_e) and a decrease (increase) in electron temperature (T_e); (c) the mixing of magnetospheric and magnetosheath plasma. Inside the magnetosphere, the plasma is hot and tenuous with low and slightly sunward velocity, whereas in the magnetosheath, the plasma is cold and dense (Marchaudon et al., 2005). Reconnection that occurs between the IMF and Earth's magnetic field lines within the lobe region is known as lobe reconnection (e.g., Frey, Phan, et al., 2003; Lockwood, 1998; Milan et al., 2022; Provan et al., 2005; Xiong et al., 2024). This process can occur independently within each hemisphere and is considered a possible cause of north-south asymmetric auroras in the polar caps (e.g., Cowley, 1981). Both spot-like HiLDAs and 15MLT-PCA are thought to result from dayside lobe reconnection occurring at high-latitude magnetopause (e.g., Cai et al., 2021; Frey, 2007; Han et al., 2020). However, this speculation currently lacks direct in-situ observations to confirm. Therefore, in this paper, we combine observations from DMSP and Cluster spacecraft to investigate the potential magnetospheric processes corresponding to the occurrence of 15MLT-PCA. We noticed that the occurrence of 15MLT-PCA was accompanied by a series of flux transport events (FTEs). A detailed analysis of these FTEs was also conducted. These findings offer direct observational evidence, confirming that 15MLT-PCA is triggered by high-latitude dayside reconnection occurring on the duskside of the cusp.

2. Data

The auroral data used in this paper are obtained from DMSP, which orbits at approximately 840 km in a sun-synchronous orbit with a period of ∼101 min (Paxton et al., 1993). The DMSP satellite, equipped with SSUSI, captures auroral emissions through scans accumulated as it passes over the polar region, providing spectral data at five wavelengths: 121.6, 130.4, 135.6, 140–150 (LBHS), and 165–180 nm (LBHL) (Paxton et al., 1993). Additionally, the satellite carries the Special Sensor J (SSJ) instrument to record the energy flux of precipitating ions and electrons ranging from 30 eV to 30 keV (Hardy et al., 1984). The Active Magnetosphere and Planetary Electrodynamics Response Experiment (AMPERE) project (Anderson et al., 2002) consists of 66 satellites distributed in six polar, low-Earth orbit (780 km altitude) planes, measuring global magnetic perturbations to calculate the distribution of field-aligned currents. The Super Dual Auroral Radar Network (SuperDARN) is a network of high-frequency (HF) radars situated in both hemispheres, spanning high and mid-latitude regions. It is designed to monitor the dynamics of the ionosphere and upper atmosphere in these latitudes, providing insights into the movement of plasma in the polar regions (Nishitani et al., 2019).

The Cluster mission conducts collaborative in-situ observations using four satellites (C1–C4) arranged in a tetrahedral formation. These satellites orbit in a polar trajectory with a perigee of approximately 4 Re and an apogee of around 19.6 Re (Escoubet et al., 2001). Each satellite is equipped with scientific instrument payloads for measuring magnetic fields, particles, and wave spectra. Among which, the Plasma Electron and Current Experiment (PEACE) measures electrons with energy ranges from a few eVs to about 30 keV (Johnstone et al., 1997), while the Cluster Ion Spectrometry (CIS) experiment analyzes ion composition and distribution in the magnetosphere using a Hot Ion Analyzer (HIA) and a CODIF instrument (Dandouras et al., 2010). During winter, Cluster passes through the lobe region of the southern hemisphere, which allows for coordinated observations with DMSP during the occurrence of 15MLT-PCA.

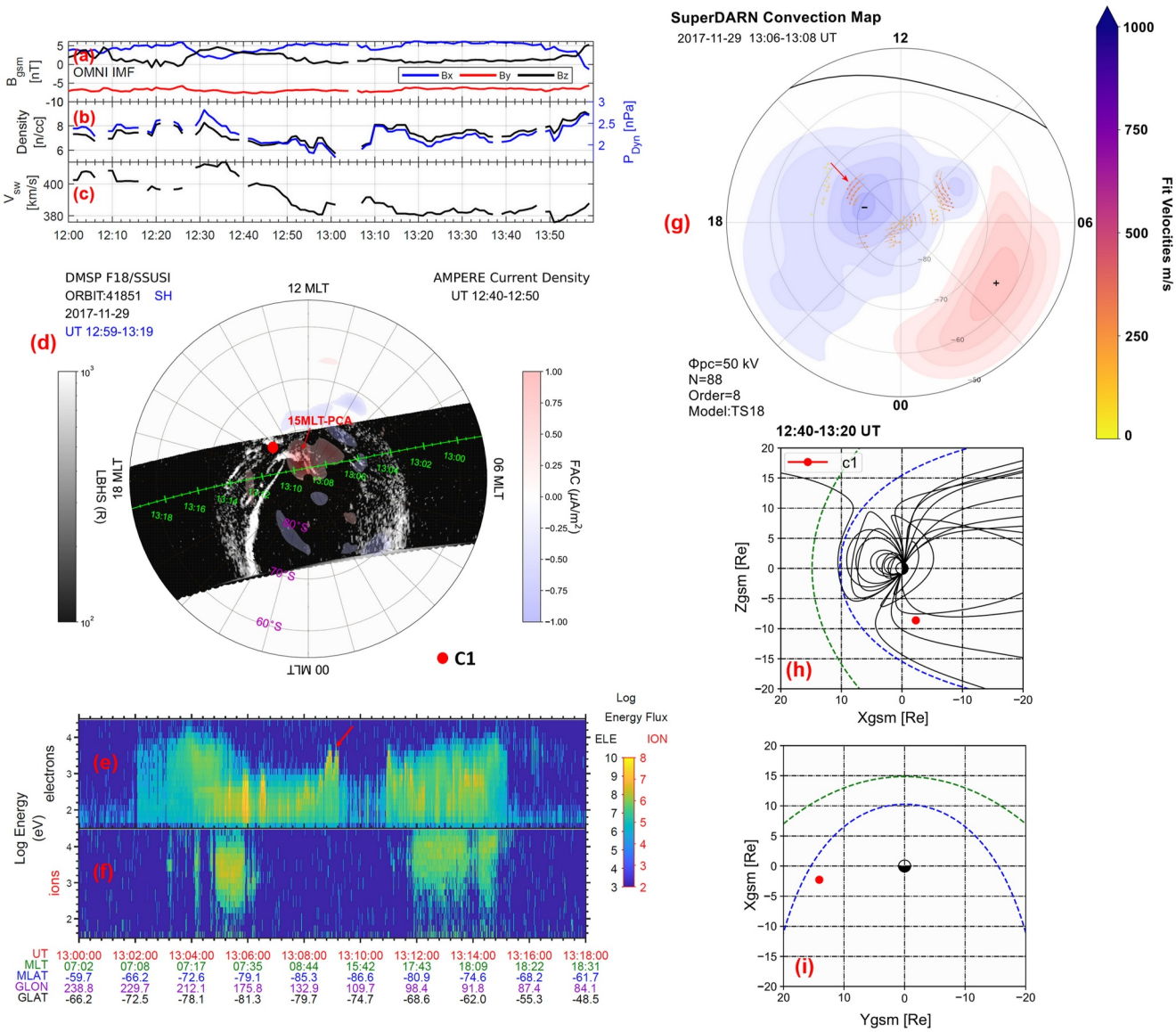

Figure 1. A 15MLT-PCA event observed on 29 November 2017. (a–c) The IMF conditions in GSM coordinate, solar wind density, dynamic pressure (P_{Dyn}), and velocity. (d) Aurora in the LBHS band from DMSP f18/SSUSI over the southern hemisphere overlaid the distribution of FACs from AMPERE. The red arrow indicates the 15MLT-PCA. The green curve is the trajectory of DMSP F18, and the dot is the footprint of C1 mapped by the T89 model. (e–f) The energy flux distribution of precipitated electron and ions. The red arrow indicates the precipitated particles within the arc of 15MLT-PCA. (g) The SuperDARN convection map during 13:06-13:08 UT. (h–i) The locations of C1 in the X–Z plane and Y–X plane from 12:40:00 UT to 13:20:00 UT. The blue dotted line shows magnetopause using the model from Shue et al. (1997), and the green dotted line shows bow shock obtained from Farris and Russell (1994).

3. Observation

3.1. Interplanetary Conditions and Auroral Observations

In this paper, we report on a 15MLT-PCA event that occurred in the Southern Hemisphere on 29 November 2017. The 15MLT-PCA was observed by DMSP/SSUSI from approximately 12:00 UT to 17:00 UT, as depicted in the Figure S1a in Supporting Information S1. During the same period, no auroral features were detected within the ~1500 MLT sectors of the Northern Hemisphere, as illustrated in the Figure S1b in Supporting Information S1. Here, we will conduct a detailed analysis of the 15MLT-PCA event observed near 13:00 UT on 29 November 2017. Figure 1 provides an overview of the interplanetary conditions and auroral observations. Throughout the time-frame, the IMF conditions in Geocentric Solar Magnetospheric (GSM) coordinates exhibited significant and stable dawnward and sunward components. The conditions include $B_x \sim 5$, $B_y \sim -7$, and $B_z \sim 1$ nT. These IMF conditions

are favorable for the occurrence of 15MLT-PCA in southern hemisphere (Feng et al., 2021). The solar wind speed is slow, varying from 400 km/s to 380 km/s, with density fluctuating between 7 and 8 cm^{-3} and a dynamic pressure of ~2 nPa. Figure 1d depicts a 15MLT-PCA event in the southern hemisphere observed by the SSUSI instrument on DMSP F18 (Strom & Iwanaga, 2005). From 12:59:00 UT to 13:19:00 UT, a clear auroral arc was observed at the 1500 MLT sector extending from the main auroral oval to the polar cap, namely 15MLT-PCA, as indicated by the red arrow. The DMSP F18 flies from dawnside to duskside and passes through the tip of 15MLT-PCA, as shown by the green curve. Figure 1d overlays the distribution of field-aligned current (FAC) from AMPERE, and the map was created using an open-source Python package called GeospaceLAB (Cai et al., 2022). There exists an enhanced stripe-like upward FAC where 15MLT-PCA appeared. Figures 1e and 1f show the energy flux distribution of precipitated electrons and ions recorded by SSJ on F18. Pure electron precipitation without ions, with energy around 10 keV, manifesting as "invert-V" structures, is observed in the tip of 15MLT-PCA (Han et al., 2020), as indicated by the red arrow in Figure 1e. Figure 1g displays the ionospheric convection map during 13:06 −13:08 UT from SuperDARN observations. The result shows that there exists a single cell convection with the enhancement of sunward plasma flows near the root of 15MLT-PCA, as indicated by the red arrow. The C1 (Escoubet et al., 2001) was in the lobe region of the southern hemisphere during this period, near the duskside magnetopause, as shown in Figures 1h and 1i. The blue dotted line indicates the magnetopause's location as calculated by the model in Shue et al. (1997), and the green dotted line shows the bow shock obtained from Farris and Russell (1994). Its footprints, as mapped by the Tsyganenko magnetic field models (T89) (Tsyganenko, 1989), are near the root region of 15MLT-PCA, depicted by the red dot in Figure 1d. The location of C1 provides a likely observational condition for examining the relationship between 15MLT-PCA and lobe reconnection.

3.2. The Magnetic Variations and Plasma Conditions Observed by the C1

Figure 2a displays the magnetic field variations observed by the fluxgate magnetometer (FGM) on the C1 from 08:00:00 UT to 14:00:00 UT. In the initial period indicated by the red bar, the C1 observed the magnetic field distribution with $B_x \sim -35$, $B_y \sim 20$, and $B_z \sim 0$ nT. This indicates that C1 is situated within the magnetosphere of the southern hemisphere. During the time interval highlighted by the blue bar, C1 observed multiple reversals of the B_x and B_y components, indicating that C1 crossed the magnetopause several times. Later, C1 enters the magnetosheath region, where B_x and B_y shift to positive (~30 nT) and negative (~−20 nT), as shown by the gray bar. In the magnetosheath region, C1 experiences multiple abrupt changes in B_x and B_y, coupled with reversals in B_z polarity, coinciding with the period of the 15MLT-PCA observed by DMSP, marked by the yellow shaded region. We further examine the details of magnetic field variations and plasma conditions observed by C1 during this period.

Figures 2b and 2c illustrate the variations in the total magnetic field and its three components in GSM coordinates. With the exception of a few notable disturbances, the magnetic fields generally remained stable, exhibiting $B_x \sim 20$, $B_y \sim -20$, and $B_z \sim 0$ nT. This pattern is consistent with the characteristics of magnetosheath magnetic fields in the southern hemisphere. Throughout this period, C1 encountered at least two instances of significant magnetic field fluctuations labeled as "1" and "2", occurring sequentially with an interval of ~20 min, as highlighted by the red arrows in Figure 2b. In both disturbances, the B_z component exhibits a bipolar characteristic, first decreasing to negative and then increasing to positive, accompanied by a strong B_y component and an overall increase in total magnetic field strength. To clearly reveal these signatures, we converted the magnetic field data and plasma velocity to the local magnetopause normal coordinate system (LMN), derived using the minimum variance analysis (MVA) method (Sonnerup & Maureen, 1998) applied to the magnetic field data observed by C1 between 13:07:30 UT and 13:08:06 UT. The unit vectors of L, M, and N in the GSM coordinate system are (0.79, −0.17, 0.58) (−0.39, 0.58, 0.71), and (−0.46, −0.79, 0.39), respectively, with corresponding eigenvalues λ of 202, 7.9, and 1.37. We converted the magnetic field and velocities from 12:40 to 13:20 UT into this coordinate system, as shown in Figures 2d–2h.

In disturbance "1", the B_N component exhibited a clear bipolar signal, transitioning from negative to positive around 12:48:00 UT. The magnitude peaks of |B|, B_L, and B_M reaches approximately 52, 51, and 25 nT, respectively, as shown in Figures 2b and 2d. Concurrently, the electron speed (V_x) turns from tailward at ~−290 km/s to earthward at ~280 km/s. This is accompanied by a reversal of V_N, a decrease in electron density from ~10 to ~6 cm^{-3}, and an increase in electron parallel temperature from ~0.4 MK (MK) to 0.6 MK, as illustrated in Figures 2e–2j. During disturbance "2", the variations in B_L, B_M, and B_N components show sinusoidal-like characteristics, initially negative and then turning positive, as shown in Figure 2d. The point of B_N

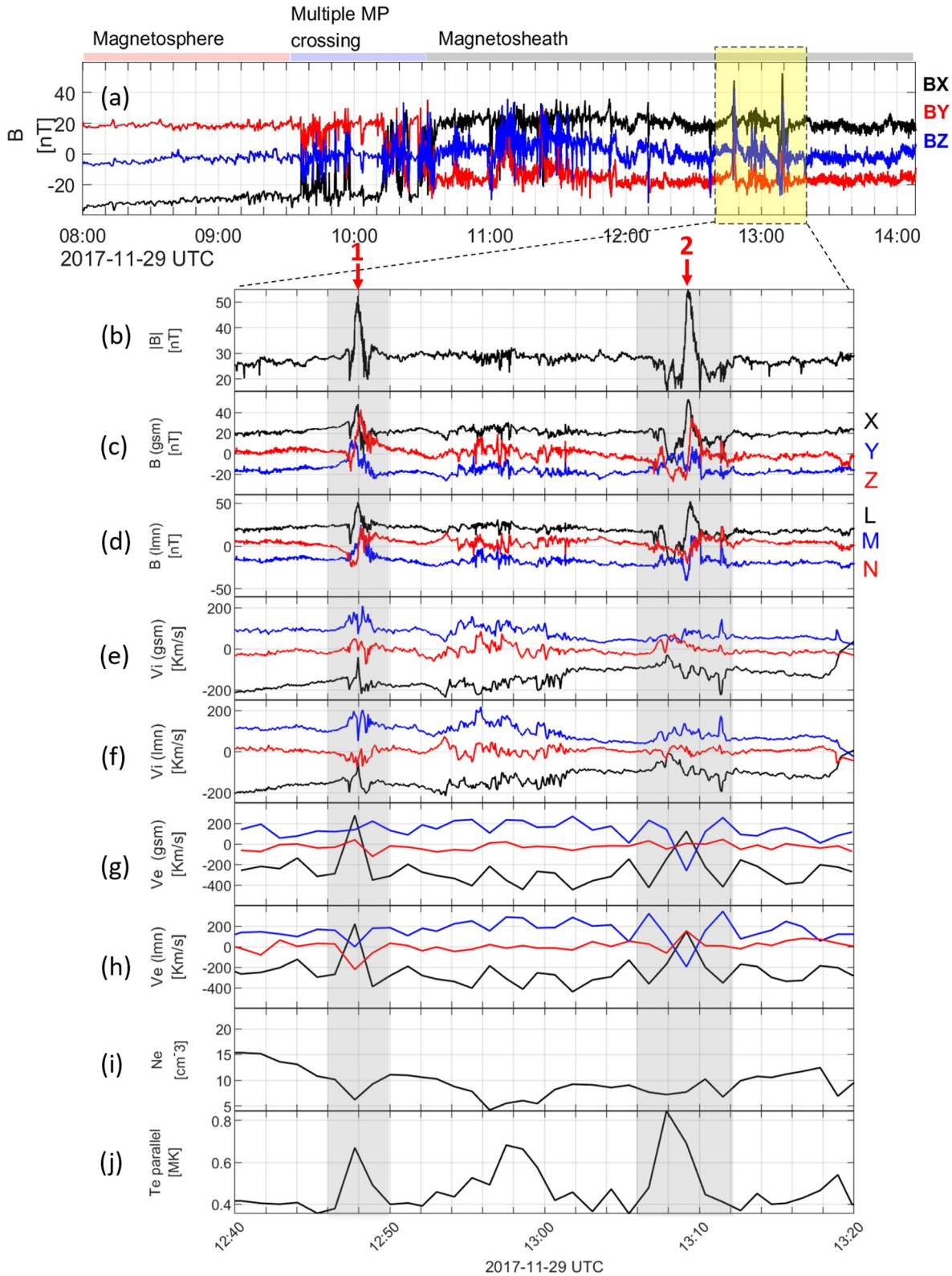

Figure 2. The variations of magnetic field and plasma parameters recorded by C1. (a) The variation of the magnetic field from 08:00:00 UT to 14:00:00 UT. (b) The magnitude of the magnetic field from 12:40:00 UT to 13:20:00 UT. (c) The X, Y, and Z components of the magnetic field in GSM coordinate. (d) The L, M, and N components of the magnetic field. (e) The X, Y, and Z components of ion velocity. (f) The L, M, and N components of ion velocity. (g) The X, Y, and Z components of electron velocity. (h) The L, M, and N components of electron velocity. (i) The density of electrons (j) The parallel temperature of electrons.

reversal ($B_N = 0$ nT) occurs around 13:09:00 UT, coinciding with peaks in |B|, B_L, and B_M at ∼54, ∼50, and ∼12 nT. A reversal in the electron V_x component shifts from tailward at ∼−400 km/s to earthward at ∼125 km/s, accompanied by V_y component reversal from duskward at ∼200 km/s to dawnward at ∼−250 km/s, as presented in Figure 2g. Additionally, a reversal from negative to positive in the L direction of electron velocity can also be observed (Figure 2h). The electron density is about 7.5 cm^{-3}, and the electron parallel temperature increases, with a peak at ∼0.8 MK, as shown by Figures 2i and 2j. The variations observed during these two disturbances are consistent with the typical characteristics of FTEs observed by satellites in the magnetosheath (Elphic et al., 1986; Retino et al., 2008; Zong et al., 2004). In the following text, we will refer to these two as FTE-1 and FTE-2 respectively.

3.3. Particle Observations From C1

We further investigated the distribution of electron and ion energy flux during the FTE-1 period, as indicated by the gray shading in Figure 3. Based on the different properties shown by the particle distribution, we divided FTE-1 into two regions, labeled by A and B. Figures 3a–3c and 3d–3f show the electron and ion energy flux distributions in the directions parallel (pitch angle (PA) = 7.5° and 5.625°), perpendicular (PA = 82.5° and 84.375°), and anti-parallel (PA = 172.5° and 174.375) to the magnetic field lines, respectively. During the FTE-1, the electrons energy varies from a few tens of eV to a few keV, while the ions exhibit distinctly different distribution characteristics in the two regions. In region A, there is a noticeable increase in ion flux in both parallel (PA = 5.625°) and perpendicular (PA = 84.375°) directions to the magnetic field lines, while a weakening trend is observed in the anti-parallel direction (PA = 174.375°), as shown in Figures 3d–3f. This is accompanied by an increase in energy from ∼1 keV to several keV. Conversely, in region B, the ion flux is notably stronger in the anti-parallel direction (PA = 174.375°) compared to the parallel (PA = 5.625°) and perpendicular (PA = 84.375°) directions. Additionally, particles in this region exhibit characteristics of both magnetosheath and magnetospheric particles, with ion energies ranging from several hundred of eV to several keV. Figures 3g and 3h illustrate the pitch angle distribution for low-energy ($E < 100$ eV) and high-energy ($E > 100$ eV) electrons of FTE-1. In region A, the flux of low-energy particles decreases, while the flux of particles with energy >100 eV increases obviously at all pitch angles, showing an isotropy distribution. In region B, the flux of low-energy electrons increases significantly in both the parallel (PA = ∼25°) and anti-parallel (PA = ∼150°) directions, exhibiting a butterfly distribution. In regions outside A and B, high-energy electrons are observed only in the anti-parallel direction (∼150°), as shown in Figure 3h. We also observed the same particle distribution in FTE-2, as presented in the Supporting Information S1.

4. Discussion

15MLT-PCA has suggested to be an auroral phenomenon occurring at the duskside of cusp in the sunlit hemisphere, and its occurrence exhibits significant dependence on the IMF B_y (Feng et al., 2021, 2022; Han et al., 2020), that is, positive B_y in the northern hemisphere and negative B_y in the southern hemisphere. Previous studies have speculated that the formation of both 15MLT-PCA and spot-like HiLDAs is most likely related to the lobe reconnection. The source region of these phenomena is likely mapped to the high-latitude region at tailward of the cusp, based on estimates of electron density distribution (Cai et al., 2021). In this paper, joint observations by DMSP and Cluster spacecraft provide direct observational evidence that the high-latitude dayside reconnection, occurring between IMF dominated by B_y component and lobe open magnetic field lines at the duskside of cusp, is responsible for the formation of 15MLT-PCA.

Figure 4 systematically depicts the possible global generation processes of 15MLT-PCA in this paper. The lobe magnetic field lines on high-latitude dusk side of cusp reconnect with the negative B_y-dominated IMF, creating FTEs. The FTEs move sunward, passing through the Cluster spacecraft. During this period, C1 encounters multiple reversal signals of IMF B_z and B_x, characterized by a sequence of changes from negative to positive in B_z and from decreasing to increasing in B_x. In LMN coordinates, the spacecraft should detect the bipolar reversal of B_N, that is, negative first and then positive in the southern hemisphere, and the enhancement of B_L and B_T accompanied by increases (decreases) and decreases (increases) of N_e and T_e (Marchaudon et al., 2005; Russell & Elphic, 1979). The observational results from C1 reflect these processes exactly, as shown in Figures 2b–2j. In both FTE events, we observed the magnetic field initially negative in the N direction, followed by a positive direction, accompanied by an increase in B_T, a decrease in N_e, and an increase in T_e. The C1 encounters the sunward electron flow slightly before the B_N reverses (Figures 2d and 2g–2h), reflecting the electron outflow after

10.1029/2024GL111793

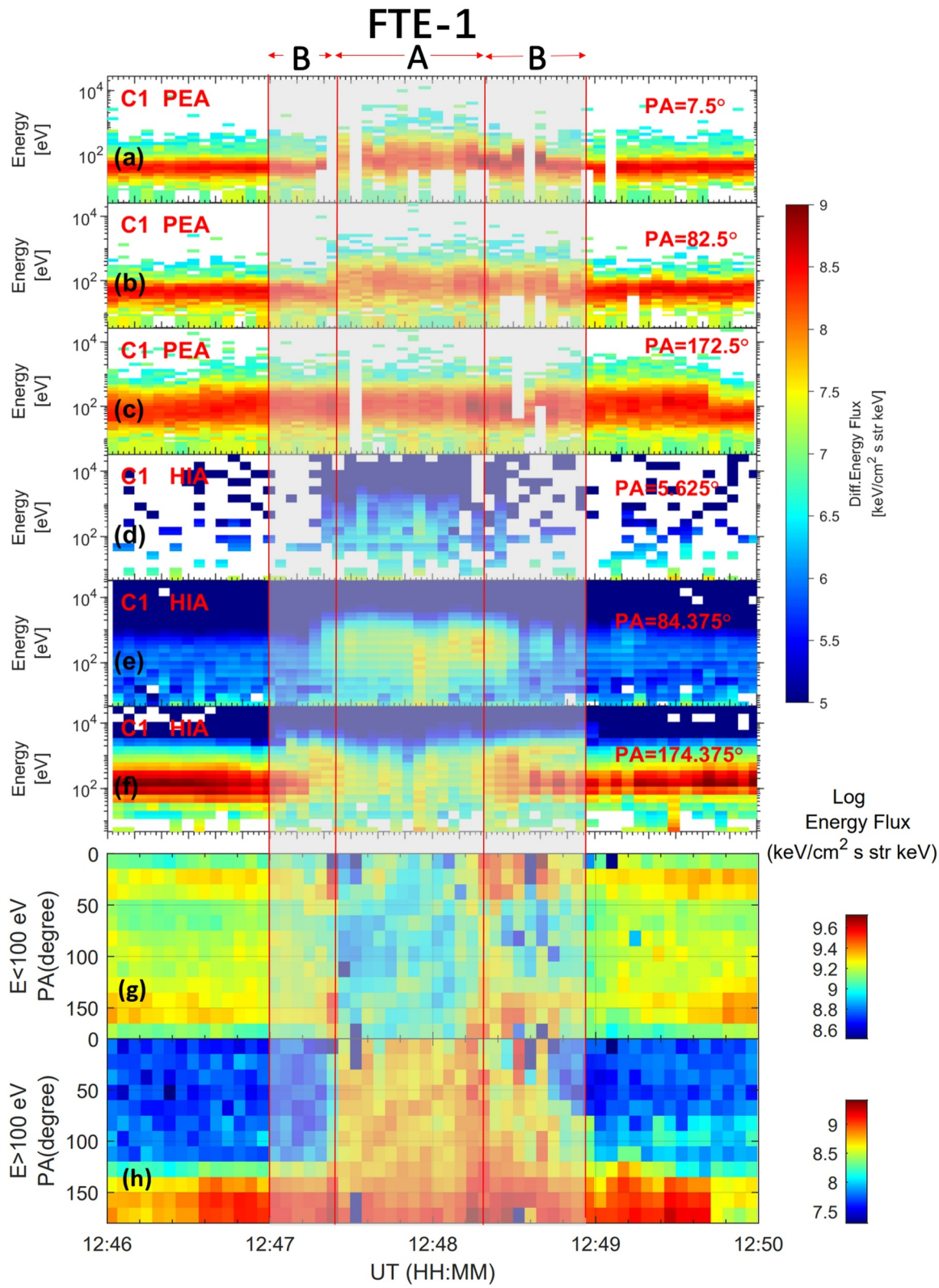

Figure 3. The distribution of electron and ion energy flux varies with different pitch angles. (a–c) The electron energy flux spectrum for pitch angle (PA) at 7.5°, 82.5° and 172.5°. (d–f) The ion energy flux distribution for PA at ∼5.625°, ∼84.375°, and ∼174.375°. (g–h) The pitch angle distributions for low-energy and high-energy electrons ($E < 100$ and $E > 100$ eV).

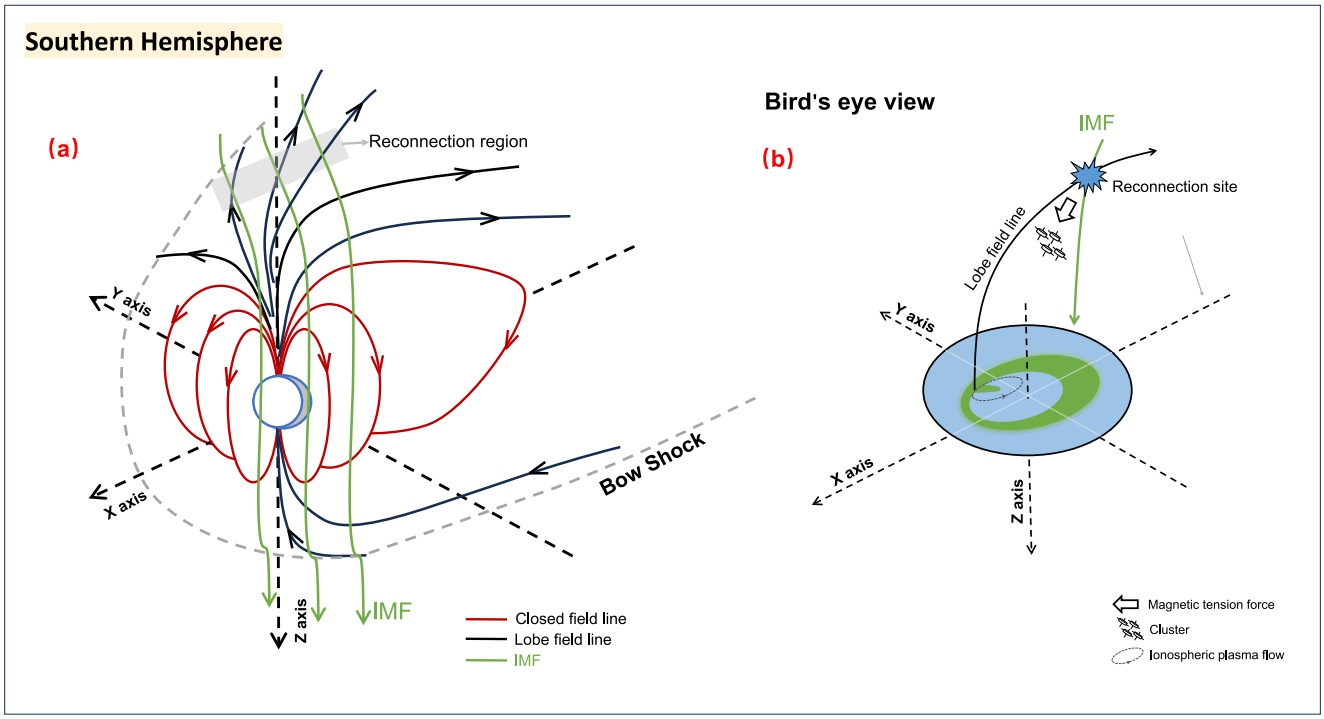

Figure 4. Schematic of formation mechanism for 15MLT-PCA. (a) The red, black and green lines indicate the closed field lines, lobe field lines, and IMF, respectively. The likely reconnection region is marked by a gray shaded. (b) A bird's eye view of the magnetic field lines associated with the 15MLT-PCA, along with the ionospheric plasma flow induced by lobe reconnection. The Cluster are positioned near the reoriented lobe open field lines.

reconnection. During the reconnection processes, electrons and ions are accelerated to higher energies (Hoshino et al., 2001; Pritchett, 2006).

In region A of FTE-1, as shown in Figures 3g and 3h, the energy flux of electrons <100 eV decreases significantly at all pitch angles, while the energy flux of electrons >100 eV increases sharply at all pitch angles. This means that these low-energy particles are accelerated to higher energies. In addition, the electron energy peaks at ∼1 keV, which is lower than the typical energy of magnetospheric electrons (>10 keV). It may imply that these electrons originate from the lobe region and are trapped on closed field lines confined within the plasmoid. The presence of trapped electrons within FTEs has been confirmed by numerous studies (e.g., Owen et al., 2001; Pu et al., 2013; Robert et al., 2006). Additionally, one of the most distinctive features of the 15MLT-PCA is that its root exhibits both electron and ion precipitation, while only electrons are observed in the arc region (Han et al., 2020). Fear et al. (2014) show electron and ion precipitation present in DMSP over the footprint of the transpolar arc, whereas the observations in this paper only show electrons in the arc; this is consistent with Newell et al. (2009) who propose three distinct types of polar cap arcs depending on their plasma properties, whereby an electron only signature is indicative of formation on open field lines. These further support the lobe reconnection suggestions discussed in the paper.

After reconnection, under the influence of magnetic tension, the newly opened field lines initially move toward the low latitudes and the morning side before eventually extending toward the tail. They induce a high-latitude ionospheric convection within the dusk circular cell driven by the Dungey cycle, manifesting as a large, round cell, as depicted by the gray dashed curved in Figure 4b. This suggestion is also supported by the SuperDARN observation in Figure 1g, where a single cell convection and an enhancement of sunward plasma flow are observed near the root of 15MLT-PCA, which can be interpreted as being caused by lobe reconnection (Reistad et al., 2021). According to the $\boldsymbol{E} = -\boldsymbol{V} \times \boldsymbol{B}$ and the high conductivity in sunlit hemisphere, these processes result in a converging electric field in the ionospheric region (Frey, 2007), forming a strong stripy-type upward FAC where the 15MLT-PCA occurs, as illustrated in Figure 1e. For northward-dominant IMF conditions, the reconnection site extend to higher latitudes and further toward the tailward of the Earth (e.g., Trattner et al., 2021). While the occurrence of 15MLT-PCA demonstrates a pronounced dependency on IMF B_y rather than B_z (Feng

et al., 2021; Han et al., 2020). It means that the reconnection site is located close to the high-latitude magnetospheric region on the duskside of the cusp. We propose that the upward current linked to 15MLT-PCA behaves more like a Region 0 field aligned current, which are associated with east-west flows in the dayside polar cap due to magnetic tension forces on newly reconnected field lines (e.g., Erlandson et al., 1988; Heikkila, 1984; Iijima et al., 1978; Ohtani et al., 1995).

5. Conclusions

In this paper, we report a typical event of 15MLT-PCA occurs in southern hemisphere, joint observed by the DMSP and Cluster. During the observation of 15MLT-PCA by DMSP/SSUSI, we noticed that Cluster, located in the lobe region with its ionospheric footprint near the root of 15MLT-PCA, encountered two FTEs with a time interval of ∼20 min, moving toward the sun. Inside the FTEs, the flux of low-energy electrons (<100 eV) decreases, while the flux of higher-energy electrons (>100 eV) increases at all pitch angles. Meanwhile, AMPERE observations show that the region where 15MLT-PCA occurs exhibits a significant increase in upward field-aligned currents. SuperDARN observed a single cell convection with an enhancement of sunward plasma flow near the root of 15MLT-PCA. These observations support that the 15MLT-PCA is caused by the reconnection between B_y-dominant IMF and the lobe open magnetic field lines at the high-latitude duskside boundary of the cusp. Further investigations into the 15MLT-PCA and FTEs in the lobe are still needed, incorporating more joint satellite and ground-based observations.

Data Availability Statement

The authors would like to thank Johns Hopkins University Applied Physics Laboratory for providing the DMSP data. The DMSP particle detectors were designed by Dave Hardy of AFRL, and data obtained from JHU/APL. The DMSP/SSUSI data can be found at https://ssusi.jhuapl.edu/data_products and DMSP/SSJ data available at http://sd-www.jhuapl.edu/Aurora/. We acknowledge use of NASA/GSFC's Space Physics Data Facility's OMNIWeb and the OMNI data can be found at https://cdaweb.gsfc.nasa.gov/index.html. We thank the AMPERE team and the AMPERE Science Center for providing the data products (https://ampere.jhuapl.edu/). We thank the ESA Cluster Active Archive for providing the data set (https://csa.esac.esa.int/csa-web/). The authors acknowledge the use of SuperDARN data. SuperDARN is a collection of radars funded by national scientific funding agencies of Australia, Canada, China, France, Italy, Japan, Norway, South Africa, United Kingdom, and the United States of America. The VT SuperDARN data is available from http://superdarn.ece.vt.edu/.

Acknowledgments
This work was supported by the National Natural Science Foundation of China (42030101, 42374191, 42204158 and 42164009) and the Shanghai Science and Technology Innovation Action Plan (No. 21DZ1206102).

References

Anderson, B. J., Takahashi, K., Kamei, T., Waters, C. L., & Toth, B. A. (2002). Birkeland current system key parameters derived from Iridium observations: Method and initial validation results. *Journal of Geophysical Research*, *107*(A6). https://doi.org/10.1029/2001JA000080

Angelopoulos, V., Artemyev, A. V., Phan, T. D., & Miyashita, Y. (2020). Near-Earth magnetotail reconnection powers space storms. *Nature Physics*, *16*(3), 317–321. https://doi.org/10.1038/s41567-019-0749-4

Cai, L., Aikio, A., Kullen, A., Deng, Y., Zhang, Y., Zhang, S.-R., et al. (2022). GeospaceLAB: Python package for managing and visualizing data in space physics. *Frontiers in Astronomy and Space Sciences*, *9*, 1023163. https://doi.org/10.3389/fspas.2022.1023163

Cai, L., Kullen, A., Zhang, Y., Karlsson, T., & Vaivads, A. (2021). DMSP observations of high-latitude dayside aurora (HiLDA). *Journal of Geophysical Research: Space Physics*, *126*(4), e2020JA028808. https://doi.org/10.1029/2020JA028808

Carter, J. A., Milan, S. E., Fogg, A. R., Paxton, L. J., & Anderson, B. J. (2018). The association of high-latitude dayside aurora with NBZ fieldaligned currents. *Journal of Geophysical Research: Space Physics*, *123*(5), 3637–3645. https://doi.org/10.1029/2017ja025082

Cowley, S. W. H. (1981). Magnetospheric asymmetries associated with the Y-component of the IMF, Planet. *Space Sci.*, *29*(79), 79–96. https://doi.org/10.1016/0032-0633(81)90141-0

Dandouras, I., Barthe, A., Penou, E., Brunato, S., Rème, H., Kistler, L. M., et al. (2010). Cluster ion Spectrometry (CIS) data in the cluster active archive (CAA). In H. Laakso, M. Taylor, & C. Escoubet (Eds.), *The cluster active archive. Astrophysics and space science proceedings*. Springer. https://doi.org/10.1007/978-90-481-3499-1_3

Dungey, J. W. (1961). Interplanetary magnetic fields and the auroral zones. *Physical Review Letters*, *6*(2), 47–48. https://doi.org/10.1103/physrevlett.6.47

Elphic, R. C., Russell, C. T., Cattell, C. A., Takahasi, K., & Bame, S. J. (1986). ISEE-1 and 2 observations of magnetic flux ropes in the magnetotail: FTE's in the plasma sheet? *Geophysical Research Letters*, *13*(7), 648–651. https://doi.org/10.1029/GL013i007p0064

Erlandson, R. E., Zanetti, L. J., Potemra, T. A., Bythrow, P. F., & Lundin, R. (1988). IMF by dependence of region 1 Birkeland currents near noon. *Journal of Geophysical Research*, *93*(A9), 9804–9814. https://doi.org/10.1029/JA093iA09p09804

Escoubet, C. P., Fehringer, M., & Goldstein, M. (2001). Introduction the cluster mission. *Annales Geophysicae*, *19*(10/12), 1197–1200. https://doi.org/10.5194/angeo-19-1197-2001

Farris, M. H., & Russell, C. T. (1994). Determining the standoff distance of the bow shock: Mach number dependence and use of models. *Journal of Geophysical Research*, *99*(A9), 17681–17689. https://doi.org/10.1029/94JA01020. issn: 0148-0227.

Fear, R. C., Milan, S. E., Maggiolo, R., Fazakerley, A. N., Dandouras, I., & Mende, S. B. (2014). Direct observation of closed magnetic flux trapped in the high-latitude magnetosphere. *Direct observation of closed magnetic flux trapped in the high-latitude magnetosphere. Science*, *346*(6216), 1506–1510. https://doi.org/10.1126/science.1257377

Feldstein, Y. I. (1990). A quarter of a century with the auroral oval. *History of Geophysics*, *4*, 103–108. AGU. https://doi.org/10.1029/hg004p0103

Feldstein, Y. I., Isaev, S. I., & Lebedinsky, A. I. (1969). The phenomenology and morphology of aurorae. *Ann. IQSY*, *4*, 311–348.

Feng, H.-T., Han, D.-S., Qiu, H.-X., Shi, R., Yang, H.-G., & Zhang, Y.-L. (2021). Observational properties of 15MLT-PCA in the Southern Hemisphere and the switching effects of IMF B_y on 15MLT-PCA occurrence. *Journal of Geophysical Research: Space Physics*, *126*(12), e2021JA029140. https://doi.org/10.1029/2021JA029140

Feng, H.-T., Han, D.-S., Teng, S.-C., Shi, R., Zhou, S., Yang, H.-G., et al. (2022). An auroral signature of the duskside boundary of the cusp. *Journal of Geophysical Research: Space Physics*, *127*(8), e2022JA030634. https://doi.org/10.1029/2022JA030634

Frey, H. U. (2007). Localized aurora beyond the auroral oval. *Review of Geophysics*, *45*(1), RG1003. https://doi.org/10.1029/2005RG000174

Frey, H. U., Immel, T. J., Lu, G., Bonnell, J., Fuselier, S. A., Mende, S. B., et al. (2003). Properties of localized, high latitude, dayside aurora. *Journal of Geophysical Research*, *108*(A4), 1–14. https://doi.org/10.1029/2002JA009332

Frey, H. U., Østgaard, N., Immel, T. J., Korth, H., & Mende, S. B. (2004). Seasonal dependence of localized, high-latitude dayside aurora (HiLDA). *Journal of Geophysical Research*, *109*(A4), 1–9. https://doi.org/10.1029/2003ja010293

Frey, H. U., Phan, T., Fuselier, S., & Mende, S. (2003). Continuous magnetic reconnection at Earth's magnetopause. *Nature*, *426*(6966), 533–537. https://doi.org/10.1038/nature02084

Han, D.-S., Feng, H.-T., Zhang, H., Zhou, S., & Zhang, Y.-L. (2020). A new type of polar cap arc observed in the ~1500 MLT sector: 1. Northern hemisphere observations. *Geophysical Research Letters*, *47*(20), e2020GL090261. https://doi.org/10.1029/2020GL090261

Hardy, D. A., Schmitt, L. K., Gussenhoven, M. S., Marshall, F. J., Yeh, H. C., Shumaker, T. L., et al. (1984). *Precipitating electron and ion detectors (SSJ/4) for the block 5D/flights 6–10 DMSP satellites: Calibration and data presentation Rep. Air Force Geophys.* Lab., Hanscom Air Force Base.

Heikkila, W. J. (1984). Magnetospheric topology of fields and currents. In T. A. Potemra (Ed.), *Magnetospheric currents*. American Geophysical Union. https://doi.org/10.1029/GM028p0208

Hoshino, M., Mukai, T., Terasawa, T., & Shinohara, I. (2001). Suprathermal electron acceleration in magnetic reconnection. *Journal of Geophysical Research*, *106*(A11), 25979–25997. https://doi.org/10.1029/2001JA900052

Hosokawa, K., Kullen, A., Milan, S., Reidy, J., Zou, Y., Frey, H. U., et al. (2020). Aurora in the polar cap: A review. *Space Science Reviews*, *216*(1), 15. https://doi.org/10.1007/s11214-020-0637-3

Iijima, T., Fujii, R., Potemra, T. A., & Saflekos, N. A. (1978). Field-aligned currents in the south polar cusp and their relationship to the interplanetary magnetic field. *Journal of Geophysical Research*, *83*(A12), 5595–5603. https://doi.org/10.1029/JA083iA12p05595

Johnstone, A. D., Alsop, C., Burge, S., Carter, P. J., Coates, A. J., Coker, A. J., et al. (1997). Peace: A plasma electron and current experiment. *Space Science Reviews*, *79*(1/2), 351–398. https://doi.org/10.1023/A:1004938001388

Kullen, A., Fear, R. C., Milan, S. E., Carter, J. A., & Karlsson, T. (2015). The statistical difference between bending arcs and regular polar arcs. *Journal of Geophysical Research: Space Physics*, *120*(12), 10. https://doi.org/10.1002/2015JA021298

Lockwood, M. (1998). Identifying the open-closed field line boundary. In J. Moen, A. Egeland, & M. Lockwood (Eds.), *Polar cap boundary phenomena, polar cap boundary phenomena*, NATO ASI Series, Kluwer Academic Publishers. https://doi.org/10.1007/978-94-011-5214-3_7

Marchaudon, A., Owen, C. J., Bosqued, J. M., Fear, R. C., Fazakerley, A. N., Dunlop, M. W., et al. (2005). Simultaneous Double Star and Cluster FTEs observations on the dawnside flank of the magnetosphere. *Annales Geophysicae*, *23*(8), 2877–2887. https://doi.org/10.5194/angeo-23-2877-2005

Milan, S. E., Bower, G. E., Carter, J. A., Paxton, L. J., Anderson, B. J., & Hairston, M. R. (2022). Lobe reconnection and cusp-aligned auroral arcs. *Journal of Geophysical Research: Space Physics*, *127*(6), e2021JA030089. https://doi.org/10.1029/2021ja030089

Newell, P. T., Liou, K., & Wilson, G. R. (2009). Polar cap particle precipi-tation and aurora: Review and commentary. *Journal of Atmospheric and Solar-Terrestrial Physics*, *71*(2), 199–215. https://doi.org/10.1016/j.jastp.2008.11.004

Nishitani, N., Ruohoniemi, J. M., Lester, M., Baker, J. B. H., Koustov, A. V., Shepherd, S. G., et al. (2019). Review of the accomplishments of mid-latitude super dual auroral radar network (SuperDARN) HF radars. *Progress in Earth and Planetary Science*, *6*(1), 27. https://doi.org/10.1186/s40645-019-0270-5

Ohtani, S., Potemra, T. A., Newell, P. T., Zanetti, L. J., Iijima, T., Watanabe, M., et al. (1995). Simultaneous prenoon and postnoon observations of three field-aligned current systems from Viking and DMSP-F7. *Journal of Geophysical Research*, *100*(A1), 119–136. https://doi.org/10.1029/94JA02073

Owen, C. J., Fazakerley, A. N., Carter, P. J., Coates, A. J., Krauklis, I. C., Szita, S., et al. (2001). Cluster PEACE observations of electrons during magnetospheric flux transfer events. *Annales Geophysicae*, *19*(10/12), 1509–1522. https://doi.org/10.5194/angeo-19-1509-2001

Paxton, L. J., Meng, C.-I., Fountain, G. H., Ogorzalek, B. S., Darlington, E. H., Goldsten, J., & Peacock, K. (1993). SSUSI: Horizon-tohorizon and limb-viewing spectrographic imager for remote sensing of environmental parameters, Ultraviolet Technology IV. *SPIEL*, *1764*, 161–176.

Pritchett, P. L. (2006). Relativistic electron production during driven magnetic reconnection. *Geophysical Research Letters*, *33*(13), L13104. https://doi.org/10.1029/2005GL025267

Provan, G., Lester, M., Grocott, A., & Cowley, S. W. H. (2005). Pulsed flows observed during an interval of prolonged northward IMF. *Annales Geophysicae*, *23*(4), 1207–1225. https://doi.org/10.5194/angeo-23-1207-2005

Pu, Z. Y., Raeder, J., Zhong, J., Bogdanova, Y. V., Dunlop, M., Xiao, C. J., et al. (2013). Magnetic topologies of an in vivo FTE observed by Double Star/TC-1 at Earth's magnetopause. *Geophysical Research Letters*, *40*(14), 3502–3506. https://doi.org/10.1002/grl.50714

Reistad, J. P., Laundal, K. M., Østgaard, N., Ohma, A., Burrell, A. G., Hatch, S. M., et al. (2021). Quantifyingthe lobe reconnection rate duringdominant IMF by periods and differentdipole tilt orientations. *Journal of Geophysical Research: Space Physics*, *126*(11), e2021JA029742. https://doi.org/10.1029/2021JA029742

Retino`, A., Nakamura, R., Vaivads, A., Khotyaintsev, Y., Hayakawa, T., Tanaka, K., et al. (2008). Cluster observations of energetic electrons and electromagnetic fields within a reconnecting thin current sheet in the Earth's magnetotail. *Journal of Geophysical Research*, *113*(A12), A12215. https://doi.org/10.1029/2008ja013511

Robert, P., Lecontel, O., Roux, A., Canu, P., Fontaine, D., Chanteur, G., et al. (2006). Study of a flux transfer event with Cluster spacecraft. In K. Fletcher (Ed.), *Cluster and double star symposium, 5th anniversity of cluster in space*. Eur. Space Agency. ESA SP-598.

Russell, C. T., & Elphic, R. C. (1979). ISEE observations of flux transfer events at the dayside magnetopause. *Geophysical Research Letters*, *6*(1), 33–36. https://doi.org/10.1029/gl006i001p00033

Shue, J.-H., Chao, J. K., Fu, H. C., Russell, C. T., Song, P., Khurana, K. K., & Singer, H. J. (1997). A new functional form to study the solar wind control of the magnetopause size and shape. *Journal of Geophysical Research*, *102*(A5), 9497–9511. https://doi.org/10.1029/97ja00196

Sonnerup, B. U. Ö., & Maureen, S. (1998). Minimum and maximum variance analysis. In G. Paschmann & P. W. Daly (Eds.), *Analysis methods for multi-spacecraft data* (pp. 185–220). ESA Publications Division.

Strom, S. R., & Iwanaga, G. (2005). Overview and history of the Defense meteorological satellite Program. *Crosslink. Aerosp. Corporation Mag. Adv. Aerosp. Technol.*, *6*, 1.

Trattner, K. J., Petrinec, S. M., & Fuselier, S. A. (2021). The location of magnetic reconnection at Earth's magnetopause. *Space Science Reviews*, *217*(3), 41. https://doi.org/10.1007/s11214-021-00817-8

Tsyganenko, N. A. (1989). A magnetospheric magnetic field model with a warped tail current sheet. *Planetary and Space Science*, *37*(1), 5–20. https://doi.org/10.1016/0032-0633(89)90066-4

Xiong, Y.-T., Han, D.-S., Wang, Z.-w., Shi, R., & Feng, H.-T. (2024). Intermittent lobe reconnection under prolonged northward interplanetary magnetic field condition: Insights from cusp spot event observations. *Geophysical Research Letters*, *51*(2), e2023GL106387. https://doi.org/10.1029/2023gl106387

Yamada, M., Kulsrud, R., & Ji, H. (2010). Magnetic reconnection. *Reviews of Modern Physics*, *82*(1), 603–664. https://doi.org/10.1103/revmodphys.82.603

Zhang, Q. H., Zhang, Y. L., Wang, C., Oksavik, K., Lyons, L. R., Lockwood, M., et al. (2021). A space hurricane over the Earth's polar ionosphere. *Nature Communications*, *12*(1), 1207. https://doi.org/10.1038/s41467-021-21459-y

Zhang, Y., Paxton, L. J., Zhang, Q.-H., & Xing, Z. (2016). Polar cap arcs: Sun-aligned or cusp-aligned? *Journal of Atmospheric and Solar-Terrestrial Physics*, *146*, 123–128. https://doi.org/10.1016/j.jastp.2016.06.001

Zong, Q.-G., Fritz, T. A., Pu, Z. Y., Fu, S. Y., Baker, D. N., Zhang, H., et al. (2004). Cluster observations of earthward flowing plasmoid in the tail. *Geophysical Research Letters*, *31*(18), L18803. https://doi.org/10.1029/2004GL020692